

# Spatial Map of Synthesized Criteria for the Redundancy Resolution of Human Arm Movements

Zhi Li, Dejan Milutinovic, *Member, IEEE*, and Jacob Rosen

**Abstract**—The kinematic redundancy of the human arm enables the elbow position to rotate about the axis going through the shoulder and wrist, which results in infinite possible arm postures when the arm reaches to a target in a 3-D workspace. To infer the control strategy the human motor system uses to resolve redundancy in reaching movements, this paper compares five redundancy resolution criteria and evaluates their arm posture prediction performance using data on healthy human motion. Two synthesized criteria are developed to provide better real-time arm posture prediction than the five individual criteria. Of these two, the criterion synthesized using an exponential method predicts the arm posture more accurately than that using a least squares approach, and therefore is preferable for inferring the contributions of the individual criteria to motor control during reaching movements. As a methodology contribution, this paper proposes a framework to compare and evaluate redundancy resolution criteria for arm motion control. A cluster analysis which associates criterion contributions with regions of the workspace provides a guideline for designing a real-time motion control system applicable to upper-limb exoskeletons for stroke rehabilitation.

**Index Terms**—Arm motion control, kinematic redundancy resolution, upper limb exoskeleton.

## I. INTRODUCTION

THE HUMAN arm is kinematically redundant with respect to reaching and grasping tasks in a 3-D workspace. As a result, an upper limb exoskeleton designed for stroke rehabilitation requires a motion control strategy that can render natural arm postures. For this purpose, this paper studies reaching movements to infer the motor control strategy used by the healthy human arm, and to apply it to the real-time motion control of the EXO-UL7 upper limb exoskeleton [Fig. 1(a)].

Conventionally, motion control has been viewed as a matter of the structure and function of the central nervous system. Studies from the perspective of neuroanatomy have focused on relating motor functions to different cortical, sub-cortical,

Manuscript received October 18, 2013; revised June 23, 2014; accepted September 23, 2014. Date of publication December 18, 2014; date of current version November 04, 2015.

Z. Li is with the Intelligent Motion Lab, Department of Electrical and Computer Engineering, Duke University, Durham, NC 27708 USA (e-mail: muyimolin@gmail.com).

D. Milutinovic is with the Department of Computer Engineering, University of California-Santa Cruz, Santa Cruz, CA 95064 USA (e-mail: dejan@soe.ucsc.edu).

J. Rosen is with the Bionics Lab, Department of Mechanical and Aerospace Engineering, University of California-Los Angeles, Los Angeles, CA 90095 USA (e-mail: rosen@seas.ucla.edu).

Color versions of one or more of the figures in this paper are available online at <http://ieeexplore.ieee.org>.

Digital Object Identifier 10.1109/TNSRE.2014.2382105

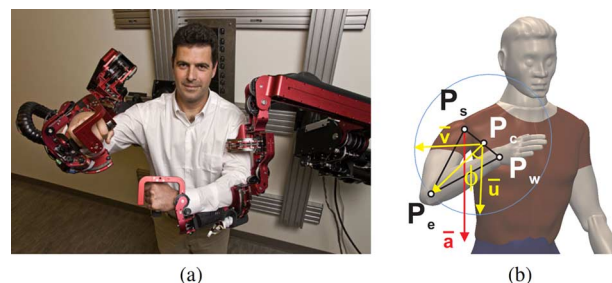


Fig. 1. (a) EXO-UL7, a dual arm exoskeleton with seven DOFs in each arm. This system exhibits kinematic redundancy identical to the human arm. (b) Given a 3-D wrist position, the arm plane formed by the positions of the shoulder ( $P_s$ ), the elbow ( $P_e$ ), and the wrist ( $P_w$ ) can move around an axis that connects the shoulder and the wrist due to kinematic redundancy. Redundant DOF can be represented by a swivel angle  $\phi$ .

and spinal subsystems [1], [2]. From the perspective of neurophysiology, Donders' law has been applied to arm postures in reaching movements, yet it is violated when pointing at a target with the elbow flexed [3]. On the other hand, the equilibrium-point (EP) hypothesis specifies physiological variables used by the central nervous system (CNS) as control variables, to address the redundancy problem (i.e., the behavior of the uncontrolled manifold) in the human motor system at the muscle level [4]. Unlike the neurophysiological perspective, a robotic viewpoint considers the human body, particularly the musculoskeletal system, as a mechanical system with kinematic and kinetic properties. The behaviors of this mechanical system are constrained by its physical structures and the laws of physics. The neural system does not so much to dictate the movement of this mechanical system as to enhance the compatibility of the system with the environment so that the task can be completed according to the requirements and with satisfactory performance [5], [6]. In this context, the redundancy of the human arm is resolved by control criteria which optimize performance variables used in mechanical engineering. Such criteria have been applied to human motor control processes such as motor planning, control, estimation, prediction, and learning [7], [8].

When executing a movement plan on a robot with redundant degrees of freedom, it is necessary to resolve the ill-posed inverse kinematics and kinetics to determine the mapping from the planned trajectory to joint motions, and then to joint torques. The problem of controlling redundant degrees of freedom (DOFs), i.e., redundancy resolution, has been considered in the control of robot manipulators. Resolution methods utilize task dependent constraints [9], [10], or more commonly, performance criteria. The latter include manipulability [11]–[14], energy consumption [3], [15], smoothness of movement

[16]–[19], task accuracy [20], and control complexity [21]. However, there is no general framework that compares and evaluates these criteria.

Redundancy resolution that synthesizes multiple movement control criteria has addressed the characteristics of movement behavior to a better extent. For instance, Miyamoto *et al.* studied reaching movements in a 2-D workspace without end-point boundary conditions. By adding a signal dependent noise to the movement controls, a linear combination of criteria maximizing the task achievement and minimizing the energy consumption resulted in a good match to the experimentally-measured hand trajectories [22]. Biess *et al.* broke down the motion control task into independent spatial and temporal motor planning. A control criterion that restricts the arm dynamics to geodesic paths is combined with a control that minimizes the squared jerk along the selected end-effector path. The resulting reaching movements in a 3-D workspace are close to those which minimize the change in joint torques and the peak value of kinematic energy [23]. Kim *et al.* studied the movements of reaching to a sequence of targets and predicted the arm postures in real-time by integrating a biological-based kinematic control criterion that maximizes the motion efficiency with a dynamic criterion that minimizes the work in joint space, showing that the kinematic criteria outperforms the dynamic one [24]. A study of the tradeoff between minimizing the angular joint displacement and averaging limits of the shoulder joint range [25] showed that a 70% – 30% linear combination of arm posture predicted by these two criteria leads to a satisfactory redundancy resolution.

From the robotic perspective, this paper proposes a general framework to compare and evaluate motion control strategies that predict arm posture in reaching movements. In this framework, the arm posture predictions of each candidate criterion are tested against experimental data collected from point-to-point reaching. By combining these candidate criteria according to their arm posture prediction accuracies, synthesized criteria are developed. The candidate criteria that better predict arm posture are assigned larger coefficients in the synthesized motion control criteria, and are therefore recognized as the ones that dominate the arm motion. For control of an upper limb exoskeleton in robot-assisted stroke rehabilitation, real-time motion control criteria are preferred, since unlike off-line motion control criteria (e.g., minimum jerk principle [17]), real-time criteria (e.g., bounded jerk criterion [26]) do not need to know about future states (e.g., the end position of the movement). Without the constraint of pre-planned movements, the upper limb exoskeleton can deal with unexpected tasks and encourages self-initiated movements on the part of the stroke patients.

In the rest of this paper, Section II describes a human arm model compatible with the EXO-UL7 upper limb exoskeleton. After introducing the real-time redundancy resolution criteria in Section III, the methods used for criterion contribution inference and the experimental protocol for data collection are presented in Section IV and Section V, respectively. According to the data analysis results in Section VI, discussion in Section VII infers the contribution of each criterion to the control of arm motion and presents a map that associates the dominant motion control strategy with different task space regions.

## II. MODELS OF HUMAN ARM

### A. Kinematic Model

The kinematic model of human arm has seven DOFs (three DOFs for the shoulder, three DOFs for the wrist and one DOF for the elbow motion). The forward kinematics, including the Denavit-Hartenberg (DH) parameters, is described in [27]. The three shoulder joint and one elbow joint are actively involved in reaching movements. As a result, the orientation of the hand in the arm model is pre-specified by locking the three DOFs at the wrist joint.

Given the wrist position in 3-D workspace, the human arm has one redundant DOF which allows the elbow to move around an axis that goes through the center of the shoulder and the wrist joints. This redundant DOF can be represented by a swivel angle  $\phi$  [see Fig. 1(b)]. Given a fixed wrist position in a 3-D workspace, the arm plane formed by the positions of the shoulder ( $P_s$ ), the elbow ( $P_e$ ), and the wrist ( $P_w$ ) can move around an axis that connects the shoulder and the wrist due to the kinematic redundancy. The direction of the elbow pivot axis (denoted by  $\vec{n}$ ) is defined as

$$\vec{n} = \frac{P_w - P_s}{\|P_w - P_s\|}. \quad (1)$$

A plane orthogonal to  $\vec{n}$  can be determined given the position of  $P_e$ . The point of intersection between the orthogonal plane and the vector  $\overrightarrow{P_w - P_s}$  is  $P_c$ .  $\overrightarrow{P_e - P_c}$  is the projection of the upper arm ( $\overrightarrow{P_e - P_s}$ ) on the orthogonal plane.  $\vec{u}$  is the projection of a normalized reference vector  $\vec{a}$  onto the orthogonal plane, which can be calculated as

$$\vec{u} = \frac{\vec{a} - (\vec{a} \cdot \vec{n})\vec{n}}{\|\vec{a} - (\vec{a} \cdot \vec{n})\vec{n}\|}. \quad (2)$$

The swivel angle  $\phi$ , representing the arm posture, is defined by the angle between the vector  $\overrightarrow{P_e - P_c}$  and  $\vec{u}$ . If the reference vector  $\vec{a}$  is  $[0, 0, -1]^T$ , then the swivel angle  $\phi = 0^\circ$  when the elbow is at its lowest possible point [28].

### B. Dynamic Model

The dynamic models of the left and right human arms are rendered via the Autolev software package [29]. The motion equations generated by Kane's method [30] integrate the estimates of mass, the center of mass, and the moment of inertia with the kinematic model of the arm. Given the initial arm condition, the dynamic model can respond to external forces (such as gravity) and provide an analytical calculation of the joint space variables (i.e., joint angles, velocities, and accelerations), as well as the kinetic energy and potential energy. When customizing the dynamic model for each individual subject, the center of mass is estimated according to the distribution of the center of mass (COM) in [31]. On average, the arm contributes 4.8% of the total body weight. The mass of arm segments and their inertia matrices are calculated based on the weight of subjects according to the regression in [32].

## III. CRITERIA FOR REDUNDANCY RESOLUTION

The EXO-UL7 exoskeleton is designed to assist self-initiated arm movements in unexpected tasks. Therefore, it requires

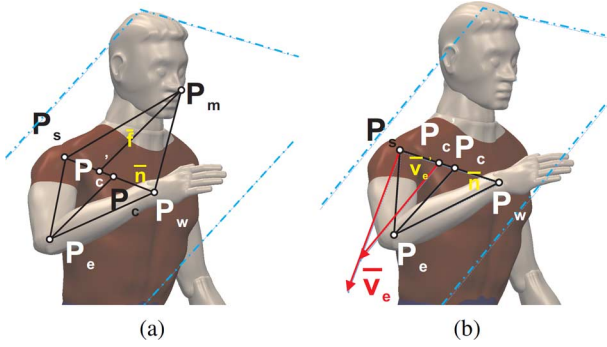


Fig. 2. (a) Criterion 1 maximizes motion efficiency by maximizing the projection of the longest principle eigen-vector of the manipulability ellipsoid on the direction from the hand to the virtual target  $P_m$ . Corresponding elbow position falls on the plane formed by  $P_s$ ,  $P_w$  and  $P_m$ . (b) Criterion 2 intends to maintain the arm posture close to the equilibrium arm posture by placing the elbow on the plane formed by the wrist position  $P_w$  and the direction of the equilibrium vector  $v_e$ .

real-time motion control rather than pre-planned motion control, and thus redundancy resolution based on local (instead of global) optimization. In this section, three kinematic and two dynamic motion control criteria are presented, which have been successful in resolving the kinematic redundancy of the human arm in reaching movements [3], [14]–[17], [33], [34]. The criteria designed for pre-planned motion control are modified as in [15] to provide real-time arm posture prediction.

#### A. Criterion 1: Maximizing the Motion Efficiency

Criterion 1 provides real-time arm posture prediction by maximizing the motion efficiency of self-feeding movements. Given the role of the head as a cluster of sensing organs and the importance of arm manipulation to deliver food to the mouth, the arm postures are determined by the human motor control system for efficiently retracting the hand to the head region. Proposed in [14], Criterion 1 determines the swivel angle by maximizing the motion efficiency to a virtual target in the head. A good candidate for the position of the virtual target is the position of the mouth, which is supported by intra-cortical stimulation experiments [35], [36]. When evoking coordinated forelimb movements in conscious primates, each stimulation site produced a stereotyped posture by which the arm moved to the same final position regardless of its posture in the initial stimulation. In the most complex example, a monkey formed a frozen pose with its hand in a grasping position in front of its open mouth, which implies that during the arm movement toward an actual target, the virtual target point at the head can be set so that the potential retraction of the hand to the mouth can be efficient.

Criterion 1 specifies a unique arm posture for each wrist position  $P_w$  in a 3-D workspace. As shown in Fig. 2(a), when the elbow falls on the plane formed by the positions of the shoulder  $P_s$ , the wrist  $P_w$  and the virtual target  $P_m$ , the projection of the longest principle eigen-vector of the manipulability ellipsoid on the direction from the hand to the virtual target  $P_m$  is maximized. In the direction of the longest principle axis of the manipulability ellipsoid, the efficiency of the velocity-force transmission between the joint space and the task space is maximized. The end-effector of the manipulator can move fastest in

this direction given the velocity inputs in the joint space. If the position of  $P_m$  is set to be the position of mouth, the designated arm postures can be the most efficient ones for self-feeding.

#### B. Criterion 2: Maintaining the Equilibrium Posture

Criterion 2, the rotational axis method proposed in [33], prefers equilibrium postures at which periarticular shoulder muscle actuation is minimized. At such postures, the upper arm is aligned with the equilibrium vector, which points out from the center of the shoulder along the axis of the circumduction cone. Criterion 2 stipulates that the axis of rotation of the arm plane (i.e., the plane formed by the positions of the shoulder, elbow, and wrist) should be the equilibrium vector. The wrist position and axis of rotation determine the arm plane which fixes the elbow position.

The direction of the equilibrium vector for the upper arm has been experimentally investigated by NASA [37]. In microgravity, the estimated shoulder flexion is about  $36^\circ$  and the shoulder abduction is about  $50^\circ$ . Given the direction of this axis, the position of the elbow always falls on the plane formed by the rotational axis  $v_e$  and the wrist position  $P_w$ . As shown in Fig. 2(b),  $v_e$  is the vector component of the rotational axis direction  $v_e$  perpendicular to  $\vec{n}$ , i.e., the vector rejection of  $v_e$  from  $\vec{n}$ . Given that  $v_e$  is parallel with the vector  $P_e - P_c$ , the swivel angle is

$$\phi = \arctan 2(\vec{n} \cdot (\vec{v}_e \times \vec{u}), \vec{v}_e \cdot \vec{u}). \quad (3)$$

#### C. Criterion 3: Minimizing Joint Angle Change

The human motor system prefers motion smoothness. Kinematic criteria that minimize the jerk in joint space and task space were proposed to account for the straight paths and bell-shaped velocity profiles observed in reaching movements [16], [17], [34], while dynamic criteria that minimize the change in joint torque [18], [19] further explained the mild curvature in the roughly straight task space trajectories. However, these available control strategies for motion smoothness are mostly designed for off-line motion control. Therefore, this paper proposes to a real-time motion control strategy based on local optimization.

Similar to Kang's minimization of the work in joint space [15], Criterion 3 determines the arm postures in the following way: given the expected positions of the wrist  $P_w(k+1)$  and the shoulder  $P_s(k+1)$ , Criterion 3 explores the possible swivel angles for the next time step  $\phi'(k+1)$  and selects the one that minimizes the norm of the change in the joint angle vector. Experimental data from [15] as well as data collected in this research show that the swivel angle never changes more than  $0.5^\circ$  per 0.01 s. Given the current swivel angle  $\phi(k)$ , Criterion 3 searches within the range of  $[\phi(k) - 0.5^\circ, \phi(k) + 0.5^\circ]$  with a step of  $\delta\phi = 0.1^\circ$ , and the swivel angle for the next time step  $\phi(k+1)$  is

$$\begin{aligned} \phi(k+1) &= \arg \min_{\phi'(k+1)} |\vec{\theta}(k) - \vec{\theta}'(k+1)| \\ &= \arg \min_{\phi'(k+1)} \sqrt{\sum_{i=1}^4 (\theta_i(k) - \theta'_i(k+1))^2}. \end{aligned} \quad (4)$$

In (4),  $\vec{\theta}(k) = [\theta_1(k), \theta_2(k), \theta_3(k), \theta_4(k)]^T$  is the joint angle vector for current time step.  $\vec{\theta}'(k+1)$  is the joint angle vector for the next time step computed from a possible  $\phi'(k+1)$  value. Since this algorithm is generally applicable to local optimization of various performance indices, in Section III-D it is also used to generate real-time control criteria that minimize kinetic energy.

#### D. Criterion 4: Minimizing the Change in Kinetic Energy

Energy-efficiency is another possible consideration. Since activities of daily living are well adapted to gravity, unless the dynamics of the human body are under additional load, the human motor system may be more concerned with the kinetic energy than potential energy. Regarding arm motion control, Soechting *et al.* suggested predicting the arm posture in reaching movements by minimizing peak kinetic energy [3]. Alternatively, Biess *et al.* minimized kinetic energy by looking for a geodesic path in the Riemannian configuration space. The resulting joint space trajectories demand less muscular effort since the sum of all configuration-speed-dependent torques vanishes along this path [23].

The aforementioned methods are for pre-planned motion control. For real-time applications, Criterion 4 determines the arm posture by local minimization of kinetic energy. With the dynamic model, kinetic energy ( $Ke$ ) for each time step is computed given the states of the arm. The algorithm described in (5) is similar to that of Criterion 3: given the kinetic energy for the current time step  $Ke(k)$ , Criterion 4 explores the possible swivel angles for the next time step  $\phi'(k+1)$  within the range of  $[\phi(k) - 0.5^\circ, \phi(k) + 0.5^\circ]$  by the step of  $\delta\phi = 0.1^\circ$ . The expected kinetic energy demanded at the next time step  $Ke'(k+1)$  is extracted from the dynamic arm model. The swivel angle that minimizes the change in kinetic energy will be selected as the swivel angle prediction for the next time step ( $\phi(k+1)$ )

$$\phi(k+1) = \arg \min_{\phi'(k+1)} |Ke(k) - Ke'(k+1)|. \quad (5)$$

#### E. Criterion 5: Minimizing the Work in Joint Space

Minimizing the work in joint space is proposed by Kang as a real-time dynamic control criterion [15]. The work in the joint space at each time step depends on (1) the joint torques and (2) the difference in joint angles, which can be extracted from the dynamic model given the states of the arm. As (6), Criterion 5 explores in the neighborhood of the current swivel angle  $\phi(k)$  and determines the swivel angle  $\phi(k+1)$  for next time step to be the one that demands the least work in joint space

$$\begin{aligned} \phi(k+1) &= \arg \min_{\phi'(k+1)} |W_i|_{t_k, t_{k+1}} \\ &= \arg \min_{\phi'(k+1)} \sum_{i=1}^4 |W_i|_{t_k, t_{k+1}}. \end{aligned} \quad (6)$$

In (6),  $|W_i|_{t_k, t_{k+1}}$  denotes the work to be done by the  $i$ th joint.

## IV. METHODS OF INFERENCE OF CRITERION CONTRIBUTIONS

The five arm motion control criteria presented in Section III account for different performance considerations,

including motion efficiency, muscle actuation efficiency, motion smoothness, and energy consumption. Their prediction performance has been tested against data collected from different experimental setups, but not against a common baseline. As a result, comparing their performance is difficult, and the relative contributions of these criteria to arm motion control have not been evaluated.

Individual contributions of different criteria inferred from experimental data provide an important guideline to coefficient assignment when combining multiple control criteria. However, methods of inferring criterion contributions have not been well explored. Kashi *et al.* inferred criterion contributions using brute-force search within a limited number of coefficient combinations [25]. This inference is neither precise enough to distinguish the behavior of different subjects, nor efficient enough to compare more control criteria within the same scale. Kim *et al.* applied least squares regression to infer the criterion contribution of the two control criteria in comparison. The inferred criterion contributions for each recorded movement are constant, which reflects behavior differences between subjects, but not how criterion contributions change during movement. In order to provide real-time inference of criterion contributions, this paper proposes (1) a modified least squares method and (2) an exponential method, both of which can compare and evaluate large numbers of criteria efficiently.

#### A. The Least Squares Method

The least squares method infers criterion contributions during a period. Considering the five candidate criteria presented in Section III, given the individual swivel angle prediction of each criterion for a time step (denoted by  $\phi_i(k)$ ,  $i = 1, \dots, 5$ ), the prediction of swivel angle for that time step (denoted by  $\phi(k)$ ) is

$$\phi(k) = \sum_1^5 c_i(k) \phi_i(k) \quad (7)$$

$c_i$  ( $i = 1, \dots, 5$ ) is the criterion contribution inferred for the  $i$ th criterion. Using recent swivel angle measurements (twenty continuous time steps in measurement history before and including the current time step), the criterion contribution of each criterion for the next time step are computed by

$$\mathbf{C}(\mathbf{k}+1)_{5 \times 1} = \mathbf{A}^{-1} \cdot \mathbf{b} \quad (8)$$

where  $\mathbf{A}$  is the prediction history from the five criteria

$$\mathbf{A} = \begin{bmatrix} \phi_{c1}(k-19) & \cdots & \phi_{c5}(k-19) \\ \vdots & \ddots & \vdots \\ \phi_{c1}(k) & \cdots & \phi_{c5}(k) \end{bmatrix}_{20 \times 5} \quad (9)$$

$\mathbf{b}$  is the measurement history

$$\mathbf{b} = \begin{bmatrix} \phi_{\text{exp}}(k-19) \\ \vdots \\ \phi_{\text{exp}}(k) \end{bmatrix}_{20 \times 1} \quad (10)$$

and  $\mathbf{A}^{-1}$  is the pseudo-inverse of matrix  $\mathbf{A}$  using the least squares method.

The coefficients that indicate the contributions are further normalized as

$$c(k+1)_i = \frac{C(k+1)_i}{\sum_{i=1}^5 C(k+1)_i}. \quad (11)$$

With reference to (7), these coefficients will be used to generate the  $k+1$ th swivel angle prediction.

Note that for the least squares method, the more criteria being evaluated the more measurements the least squares method requires to render the estimation for current time step. The precision of the inference can be improved by involving more measurements from previous time steps. However, as the older measurements are involved, the inferred contributions become less sensitive to the temporal variation of the criterion contributions. As a result of this tradeoff, this paper tentatively proposes using the last twenty measurements when inferring the contributions by the least squares method. In experimental data, a typical trial in the reaching movement experiments lasts for 150–250 time steps at the sampling rate of 100 Hz.

### B. The Exponential Method

An alternative method of inferring contribution is the exponential method [38]. This method evaluates the contribution coefficient of a criterion based on the difference between the experimentally recorded swivel angle  $\phi_{\text{exp}}(k)$  and the swivel angle predicted by this criterion. At time step  $k$ , each of the five candidate criteria ( $i = 1, 2, \dots, 5$ ) provides an individual swivel angle prediction, denoted by  $\phi_i(k)$ . The norm of the prediction error for each criterion is computed as

$$\varepsilon_i(k) = |\phi_{\text{exp}}(k) - \phi_i(k)|. \quad (12)$$

Based on the five prediction errors, the standard deviation among the prediction errors (denoted by  $\hat{\sigma}(k)$ ) can be computed.

According to the principle of maximum entropy, the probability of the criterion  $i$  can be expressed as

$$p_i = c \cdot \exp(-\lambda \varepsilon_i^2) \quad (13)$$

(see Section IV-A). Since the maximum entropy principle does not result in the probability distribution providing bias towards any model, the experimental outcomes from all the models are assumed possible. Therefore, the standard deviation of the prediction errors  $\hat{\sigma}$  is the property shared among the models, which results in the criterion contribution  $c(k+1)_i$  computed as

$$C_i(k+1) = \exp\left[-\frac{\varepsilon_i^2(k)}{\hat{\sigma}^2(k)}\right]. \quad (14)$$

The criterion contributions are then normalized

$$c(k+1)_i = \frac{C_i(k+1)}{\sum_{i=1}^5 C_i(k+1)} \quad (15)$$

which will be used to generate the swivel angle prediction at time step  $k+1$ .

Because it does not rely on as much history, the exponential method is expected to outperform the least squares method for real-time contribution inference, particularly when the contributions of various criteria change during movement. Furthermore,

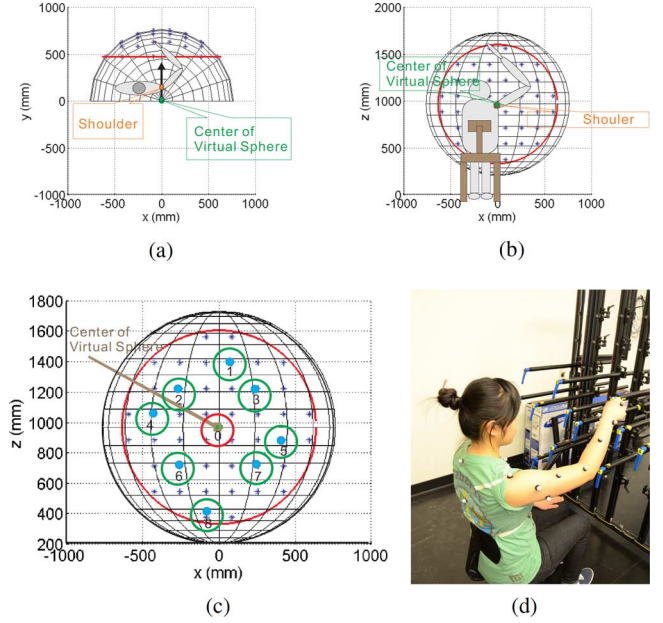


Fig. 3. (a) and (b) Top and front views of the spherical workspace, respectively. (c) Eight targets are selected among all the available targets (denoted by blue dots in circles). (d) Subject is performing the instructed reaching movements, with markers attached to her right arm and the torso for position tracking. (a) Top View. (b) Front View. (c) 3-D spherical workspace. (d) Attached markers.

the exponential method has no limit on number of the criteria it can process in parallel.

### C. Criterion Synthesis

The two proposed methods infer criterion contributions in real-time, which can be used to compare the candidate criteria. These inferred contributions can also be used as coefficients for criterion synthesis to improve arm posture prediction accuracy, because no individual control criterion can fully account for arm postures in reaching movements.

Arm motion control is adapted to various environmental constraints and is therefore subject more than one performance consideration. Synthesizing multiple control criteria takes this complexity into account. The contribution-inference/criterion-synthesis methods presented here are not limited to the five candidate criteria presented in Section III. Instead, these methods are proposed as general frameworks for control criteria comparison and evaluation. By inferring the contributions of different control criteria, a limited number of “major” components that are significant to the motor control strategy will be distinguished from the “minor” components that are less prominent considerations in arm motion control. The synthesized arm motion control criteria aim to capture the important factors that influence the motor control system, rather than generate good arm posture predictions by over-fitting the experimental data with too many variables.

## V. EXPERIMENT PROTOCOL

The arm posture predictions of motion control criteria are tested against experimental data collected on point-to-point reaching movements. In this experiment, ten healthy subjects (six males and four females) are instructed to conduct reaching

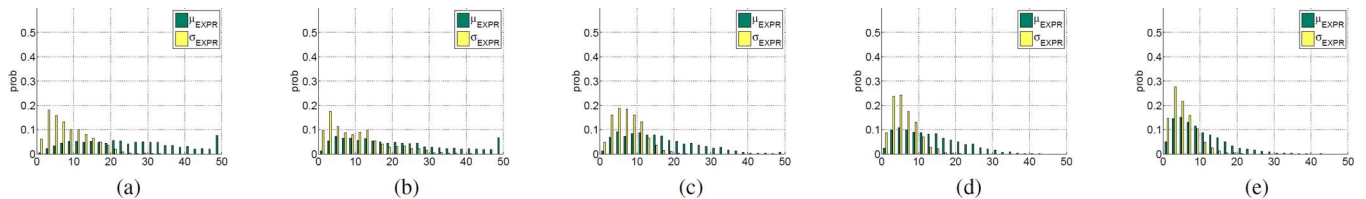


Fig. 4. Swivel angle prediction performance for each candidate criterion.  $\mu$  and  $\sigma$  denote the mean and the standard deviation of the prediction error. (a) Criterion 1. (b) Criterion 2. (c) Criterion 3. (d) Criterion 4. (e) Criterion 5.

movements with their right arms to each of the eight targets specified in the spherical workspace (Fig. 3). Each subject performs eight reaching movement sessions, one for each target. The reaching movements in each session start from one of the remaining seven targets. A complete session consists of five repetitions of seven different movements. The total number of trials for each subject is  $8 \times 7 \times 5 = 280$ . During the experiment, the subject sits in a chair with a straight back. The chair is placed such that the subject can point at the targets with comfort and with his/her elbow naturally flexed. The height of the workspace center is adjustable and is always aligned with the right shoulder of the subject. The subject's right arm is free for reaching movements, but the body of the subject is set against the chair back to minimize shoulder displacement. During the reaching movements, subjects keep the pointing fingers in line with the forearm to minimize wrist flexion.

Subjects are asked to point with the index finger tip at a comfortable pace. At the beginning of each trial, the subject is informed of the targets that the trajectory starts with and ends at, i.e., the start and end targets. After receiving a “start” command, the subject moves his/her index finger from the start target to the end target. A motion capture system records a single file for each trial at a sampling rate of 100 Hz. As shown in Fig. 3(d), passive reflective markers are attached to the torso and the right arm of the subject. The recording starts from the time when the subject points the index finger to the start target and ends after the index finger tip becomes steady at the end target. To minimize the effect of fatigue, subjects take a rest after completing each session. With the recorded data of shoulder, elbow, and wrist positions, the swivel angles profiles are extracted for each trial.

## VI. RESULTS

This section presents the results of the arm posture prediction performance of the five candidate criteria, as well as the performance of the synthesized criteria using the least squares and exponential methods. The comparison shows that the least squares method results in prediction performance comparable to the candidate criteria with good prediction performance, while the exponential method infers the criteria contribution more accurately and therefore generates much better arm posture predictions. Further data analysis clusters the computed coefficients to identify characteristic combinations of motion control criteria. The dominant regions of each characteristic combination are presented in a map that associates the clusters with wrist positions in task space.

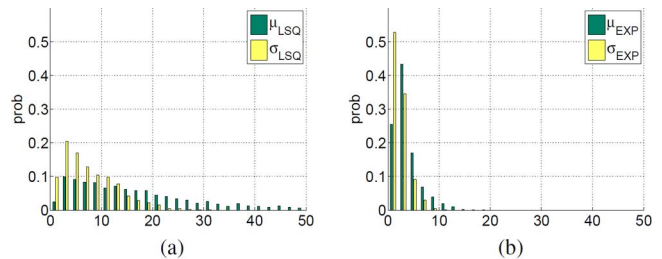


Fig. 5. Swivel angle prediction performance of the synthesized criteria using (a) the least squares method and (b) the exponential method.  $\mu$  and  $\sigma$  denote the mean and the standard deviation of the prediction error. (a) Least squares method (LSQ). (b) Exponential method (EXP).

### A. Prediction Performance of the Criteria

Figs. 4 and 5 show the means ( $\mu$ ) and standard deviations ( $\sigma$ ) of the prediction errors for all the valid trails (2674 out of 2800) conducted by 10 subjects. Fig. 4 shows the prediction performance of the five candidate criteria. Fig. 5 shows the prediction quality of the synthesized criteria using the least squares method and the exponential method, respectively. Comparison between Figs. 5 and 4 shows that the predictions of the synthesized criteria using least squares is more accurate than Criterion 1 and 2, comparable to Criterion 3 and 4, and worse than Criterion 5, while the synthesized criteria using the exponential method is much more accurate than any candidate criterion. For the exponential method, 79.32% of the trials have both  $\mu_{\text{exp}} \leq 5^\circ$  and  $\sigma_{\text{exp}} \leq 5^\circ$ , and only 3.37% trials have either  $\mu_{\text{exp}} \geq 10^\circ$  or  $\sigma_{\text{exp}} \geq 10^\circ$ . For the least squares method, 15.78% of the trials have both  $\mu_{\text{LSQ}} \leq 5^\circ$  and  $\sigma_{\text{LSQ}} \leq 5^\circ$ . 71.20% trials have either  $\mu_{\text{LSQ}} \geq 10^\circ$  or  $\sigma_{\text{LSQ}} \geq 10^\circ$ .

The exponential method infers the variance of the criterion contributions better than the least squares method. As shown in Fig. 6, the contribution coefficients assigned by the exponential method vary more than the those assigned by the least squares method. In Fig. 6, the swivel angle and the coefficients were normalized relative to the percentage of the path length traversed by the hand (instead of time), since in the reaching experiments each subject moved at his/her own pace. The coefficients corresponding to the candidate criteria are denoted by  $c_i$ , where  $i = 1, 2, 3, 4, 5$ . “Exp” denotes the measured (experimental) swivel angle profiles, and “Est” denotes the swivel angle predicted (estimated) by the synthesized criteria. Although both methods for inferring criteria contribution coefficients result in the predictions that follow trends of the measured swivel angle, the prediction errors of the exponential method are much smaller. This may be because the exponential method uses the most recent data sample, while the least square method depends on the last

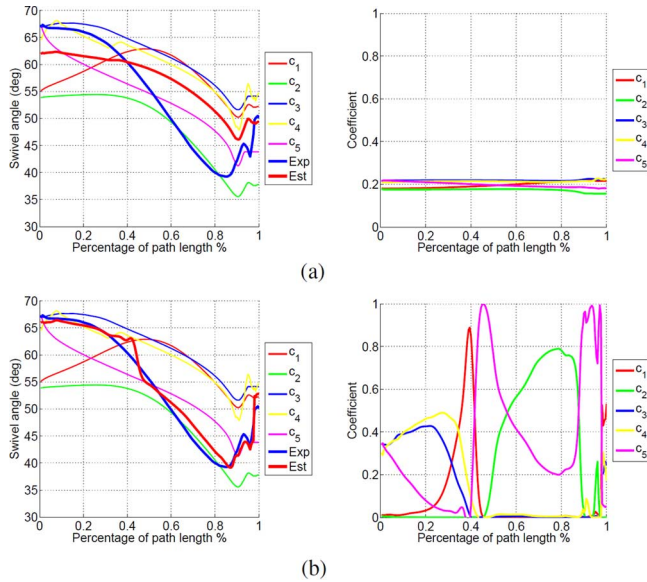


Fig. 6. Swivel angle predictions of candidate criteria, as well as their inferred contributions.  $c_1$  to  $c_5$  refer to the candidate criteria. Est refers to the synthesized criteria. Exp refers to the swivel angle measurements. (a) Least squares method (LSQ). (b) Exponential method (EXP).

20 data samples. Comparison of the coefficient profiles shows that the criteria with large prediction errors are suppressed efficiently by the exponential method, which result in a bigger spread of coefficient  $c_i$  values.

### B. Characteristic Combinations of Motion Control Criteria

The previous subsection has shown that healthy reaching movements can be best explained by synthesizing multiple criteria using the exponential method. The coefficient assigned to each criterion indicates the time-varying contribution of that criterion. In the following section, K-means clustering will be applied to the contribution coefficients inferred by the exponential method to identify the characteristic combinations of motion control criteria, which can be further mapped to task space the wrist positions.

1) *K-Means Clustering of Coefficient Vectors*: For each step during the movement, the exponential method has inferred the criterion contribution coefficients, which forms coefficient vectors  $v = [c_1, \dots, c_5]^T$ . Regardless of the sequences of consecutive steps, each coefficient vector is considered as an individual data point in the K-means clustering. In order to decide the number of clusters, the sum of the squared distances from each point to the center of its cluster (denoted by  $s_N$ ) is computed. This sum  $s_N$  decreases as the number of clusters increases. Fig. 7 shows the normalized  $s_N$  with respect to  $s_1$  for  $N = 1, 2, \dots, 20$ . At  $N = 9$ , the ratio between  $s_N$  and  $s_1$  is reduced to 5%, which is appropriate for clustering. The percentages of vector coefficients in each cluster for  $N = 9$  is shown in Fig. 7(b). Cluster 1 has about 30% of the coefficient vectors, while the population in every other cluster is less than 15%.

2) *Results of K-means Clustering*: Shown in Fig. 8(a)–(i), the K-means clustering of the coefficient vectors has identified characteristic combinations of contribution coefficients. With five candidate criteria, a threshold coefficient value of 0.2 is set

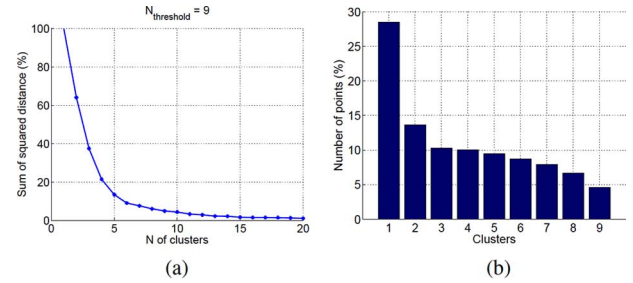


Fig. 7. Sum of the squared distances to the cluster centroid ( $s_N$ ) is computed for increasing cluster number ( $N$ ). When the ratio between  $s_N$  and  $s_1$  is reduced to 5%, the clustering is stabilized, at  $N = 9$ . (a) Clustering threshold. (b) Cluster distribution,  $N = 9$ .

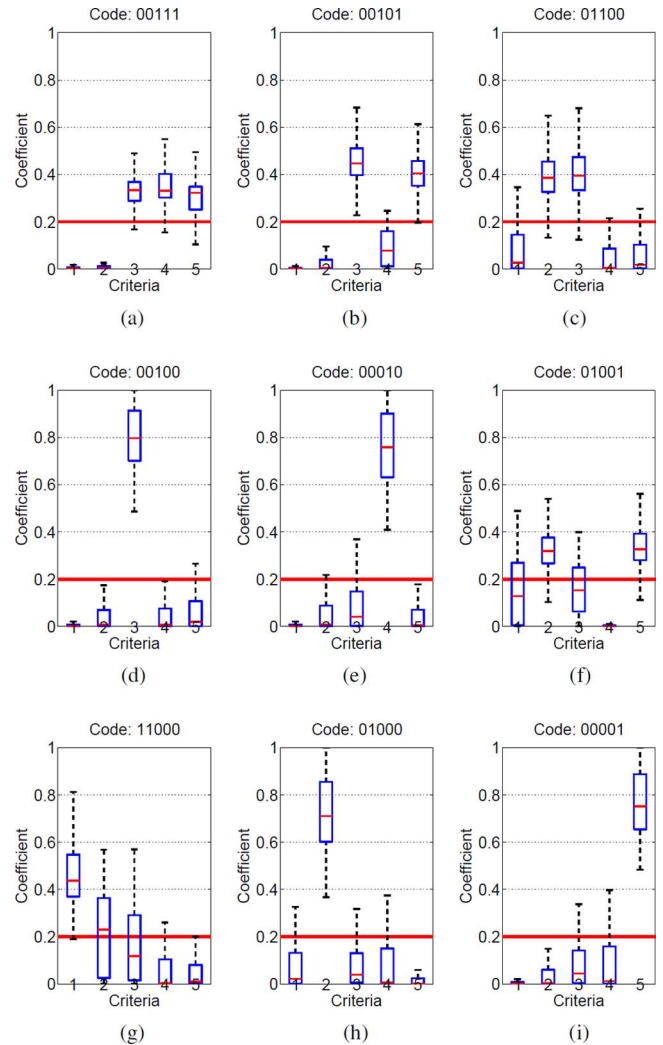


Fig. 8. Characteristic combinations of contribution coefficients are identified by K-means clustering. With respect to the threshold coefficient value 0.2, the dominant criteria are distinguished from the non-dominant ones. (a) Cluster 1. (b) Cluster 2. (c) Cluster 3. (d) Cluster 4. (e) Cluster 5. (f) Cluster 6. (g) Cluster 7. (h) Cluster 8. (i) Cluster 9.

to distinguish between the dominant and nondominant criteria. As a result, the characteristic combination of coefficients can be encoded a five digit binary string. For instance, the characteristics of movements in Cluster 1 [see Fig. 8(a)] can be encoded as 00111, indicating that Criteria 3, 4, and 5 are the dominant criteria, whereas Criteria 1 and 2 make no significant contribution.

In Fig. 8, the clusters are ordered by point populations. Clusters 1, 2, 3, and 6, which in total have about 70% of the point population, are dominated by multiple criteria, while each of the remaining five clusters has only one dominant criterion. This explains the higher performance of the synthesized criteria: most of the data can only be predicted using multiple criteria. It also explains how individual criteria can have good prediction performance in some cases: some parts of the data are best explained by a single criterion.

3) *Associating Clusters With Task Space Wrist Positions:* The clusters of coefficient vectors, which indicate the characteristic combinations of motion control criteria, can be mapped to wrist position in the task space. As shown in Fig. 9(a)–(i), the 3-D task space is divided into cells with a  $50 \times 50$  mm grid on the plane the subject is facing (i.e., the x-z plane). Every data point (i.e., coefficient vector) falls into a cell according to its associated wrist position. The frequency of a cluster in a cell is the ratio between the number of points from that cluster within that cell and the total number of points in that cell. Given a specific cluster that represents a characteristic combination of criteria, arm postures are more accurately predicted by that cluster in the regions where it has higher frequency.

Clusters 1, 2, 3, and 6 correspond to characteristic combinations with multiple dominant criteria. For instance, the dominant criteria of Cluster 1 minimize the joint angle change, the kinetic energy and the work in joint space. In Fig. 9(a), Cluster 1 has high frequency in the lower half of the task space, and in the top-right corner. Cluster 2 is like Cluster 1 except that it does not minimize kinetic energy. It only has high frequency in the lower-right of the task space. Both Clusters 3 and 6 are dominated by the rotational axis criterion. Cluster 3 also minimizes the joint angle change and works best in the top-left of the task space, while Cluster 6 also minimizes the work in joint space and works best when the wrist is on the left side of the task space.

The remaining clusters correspond to the combinations dominated by single criteria. As a result, their frequency graphs indicate the task space regions in which individual criteria have good arm posture prediction. Cluster 4 minimizes the change in joint angle and works best for the right side of the task space. Cluster 5 minimizes the kinetic energy and works well in the lower left of the task space. Cluster 7 emphasizes Criterion 1 and has high performance predicting arm posture when the hand reaches the leftmost edge of the task space or moves around the top-right of the task space. Cluster 8 is dominated by only the rotational axis method and works well for the top half of the task space. Cluster 9 minimizes the work in joint space and works best for the top-right and bottom-left regions.

Fig. 9(j) is a combination of the individual frequency graphs. In Fig. 9(j), each cell in the task space is filled with the color of the cluster with the highest frequency in that region. This colored map reflects the most frequent combinations of criteria in different regions of the task space.

## VII. DISCUSSION

This paper has analyzed recorded data from reaching movements and inferred the contributions of various criteria to arm

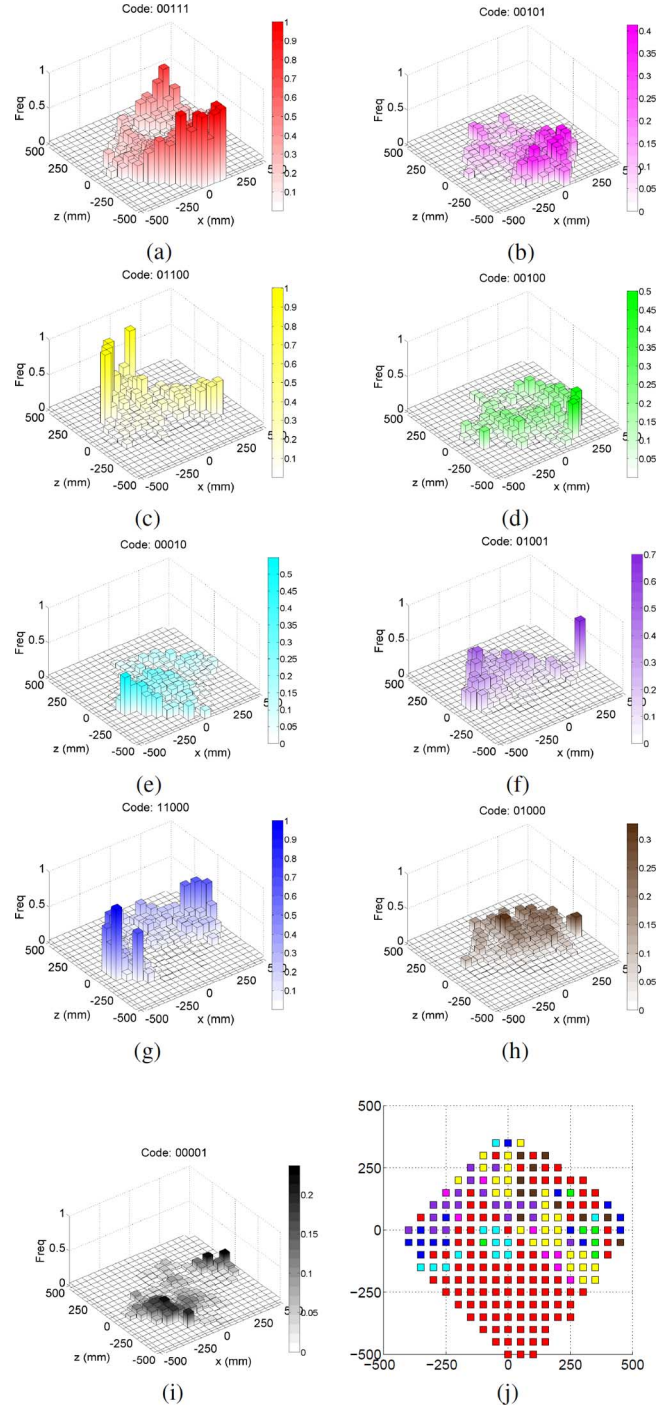


Fig. 9. Images (a)–(i) present the clusters' frequencies in the task space. Image (j) compares the graphs for the nine clusters and illustrates the most-frequent combination of motion control criteria for each cell in the task space. (a) Cluster 1. (b) Cluster 2. (c) Cluster 3. (d) Cluster 4. (e) Cluster 5. (f) Cluster 6. (g) Cluster 7. (h) Cluster 8. (i) Cluster 9. (j) Color Map.

motion control. Five criteria (three kinematic and two dynamic) are investigated, and are compared by their the swivel angle prediction performance. Inference based on synthesized criteria using the exponential method predicts the arm postures more accurately than inference using the least squares method. Using the exponential method, among 2674 valid trials collected from ten healthy subjects, the mean and standard deviation of the prediction errors during movement was less than  $5^\circ$  for 79% of the

trials, and only 3% of trials had either a mean or standard deviation of the prediction error of more than  $10^\circ$ .

Using K-means clustering, the contribution coefficient vectors are grouped into nine clusters with distinguishable coefficient value distributions, which indicate the characteristic combinations of motion control criteria. The clusters are mapped to wrist positions in the 3-D workspace, and their high-frequency regions are presented in a colored map. Based on the results presented in Section VI, this section will provide further discussion that highlights the new findings regarding the strategies of healthy arm motion control. Both the methodology contribution (i.e., the general framework that synthesizes, evaluates, and compares motion control criteria that resolve the kinematic redundancy of human arm) and its application to the real-time control of an upper limb exoskeleton will be addressed.

#### A. Regional Motion Control Strategies in the Task Space

The data analysis has shown by synthesizing a limited number of control criteria that address different aspects of motion characteristics, the kinematic redundancy of the human arm can be resolved to render natural human arm postures in reaching movements. The redundancy resolution according to the combined control criteria outperforms all of its individual components. The method used to combine the criteria is critical to getting good estimations of arm posture. The arm postures are not well-predicted by the least squares method, which assigns the contribution coefficients based on the overall prediction performance within a relatively long history. The higher performance of the exponential method, which assigns contribution coefficients only based on the prediction of the last time step indicates that the contribution of each individual criterion is time-sensitive. Indeed, the contribution coefficient assigned to each individual criterion varies during the reaching movement, instead of maintaining a constant value for the whole movement. In previous research, Kashi *et al.* integrated two kinematic control criteria and suggested constant partial contributions to combine these two criteria: 70% for the criterion that minimized angular displacement and 30% for the criterion that averaged the limits of the shoulder joint range [25]. Kim *et al.* combined a criterion that maximized motion efficiency (Criteria 1) with one that minimized the work in joint space (Criteria 5) using least squares and claimed that the contribution of the dynamic criterion is negligible compared with the kinematic criterion [14]. Biess *et al.* suggested a global path planning method that defines the temporal properties of the movement by minimizing the squared jerk along the selected end-effector path, and the spatial properties of the movements by finding the geodesic path in joint space [23]. According to this method, there exists a single control criterion that dictates the spatiotemporal properties of reaching movements. These results are all challenged by our findings that 1) the contribution coefficients of combined criteria should be time-varying instead of constant, and 2) no single control criterion can accurately model arm movements from the beginning to the end.

Clustering the contribution coefficient vectors showed the spatial dependence of the criterion contributions in addition to its temporal dependence. A combined map of cluster frequency

[Fig. 9(j)] shows that the lower part of the workspace is dominated by cluster 1 (represented by red). Cluster 1 is significantly affected by criteria 3, 4, and 5: the kinematic criterion that minimizes the joint angle change, as well as the two dynamic criteria that minimize the change in kinetic energy and the work done in joint space. A possible explanation for the high frequency of Cluster 1 in this region is that when reaching for targets in the lower part of the workspace, the arm is far away from the center of the stereoscopic visual range. Without seeing the movements of the whole arm, motion control may be more dependent on proprioceptive feedback. Low elbow postures in accordance with the direction of gravity do not block the view for reaching movement in this region, and therefore may be preferred for less energy consumption. In addition, when reaching to the lower-left part of the workspace, these energy-saving elbow postures may be preferred since the arm motion range is constrained by the torso.

In the upper-right part of the workspace, Cluster 3 is the most frequent [represented by yellow in Fig. 9(j)]. According to Fig. 8(c), the control strategy of cluster 3 is strongly affected by two kinematic criteria: maintaining the equilibrium posture (criterion 2) and minimizing the joint angle change (criterion 3). With the shoulder position aligned with the center of the workspace, the upper part of the workspace is about even with eye-level. The equilibrium posture may be preferred since it naturally brings the hand into the stereoscopic visual range, and results in less work for the periarticular muscles. Note that the dynamic model used simulates the human arm as linked rigid bodies. Without simulating muscular forces, dynamic criteria are less useful than the equilibrium posture criterion in predicting motions in this area. The criterion that minimizes the joint angle change demonstrates a strong impact in Clusters 1 to 4. Considering the fraction of the coefficient vectors in these four clusters (62.56%) and the area of the workspace where they have high frequency [see Fig. 9(a)–(d)], this criterion that emphasizes smoothness of motion is generally applicable to the whole workspace.

#### B. Methodology Contribution

As a methodology contribution, this paper proposes: 1) a general framework for the comparison of real-time motion control criteria and 2) methods for criterion synthesis and contribution inference. By synthesizing a highly-accurate motion control criterion out of several candidate criteria, the method followed here is able to infer the contribution of each candidate criterion to arm motion control, and the temporal and spatial variation of its contribution. Clustering is used to determine which criteria are related, and find characteristic combinations of criteria that best explain arm motion in different areas of the task space. This allows for high-fidelity analysis of the criterion contributions, and a computationally efficient cost function which ignores criteria with negligible contributions could be constructed as a result. This framework could also be used to evaluate more candidate criteria besides those presented in this paper.

Within the proposed general framework, the least squares and the exponential methods are investigated. Section VI-A presents the prediction quality of the synthesized criteria using these methods, as well as the prediction quality of each candidate

criterion. Compared to the least squares method, the proposed exponential method is preferable for criterion synthesis and contribution inference: it predicts the arm posture more accurately than all of the individual candidate criteria, while the least squares method predicts no better than the criterion with the best individual performance. The main difference between the two synthesis methods is that the least squares method considers the last 20 steps of history and tries to find a set of constant coefficients which maximize prediction accuracy during that period, whereas the exponential method only considers prediction error in the last step and adjusts the coefficients at each step accordingly. The least squares method would be able to predict arm posture accurately if the contribution of each candidate criterion were relatively constant, but the more accurate prediction rendered by the exponential method shows that the contributions of candidate criteria are not constant. As shown in Fig. 6–Fig. 9(j), the contribution coefficients vary in time and space.

#### APPENDIX

The entropy  $H(k)$  of the discrete probability distribution  $p_i(k)$  ( $i = 1, 2, \dots, N$ ) at the time step  $k$  is

$$H(k) = \sum_{i=1}^N p_i(k) \ln p_i(k). \quad (16)$$

The distribution satisfies the constraint

$$\sum_{i=1}^N p_i(k) = 1. \quad (17)$$

Furthermore, based on the observed quantities, the variance of the distribution should be equal to the experimentally observed variance, that is

$$\sum_{i=1}^N \varepsilon_i^2(k) p_i(k) = \hat{\sigma}^2. \quad (18)$$

According to the maximum entropy principle [38], the least informative prior distribution is defined by the set of values  $p_i(k)$  that maximize the entropy [(16)] under the above two constraints. This maximization problem can be solved using Lagrange multipliers  $\lambda_1$  and  $\lambda_2$  as an unconstrained maximization problem of the cost function  $J$

$$J = \sum_{i=1}^N p_i(k) \ln p_i(k) - \lambda_1 \left( \sum_{i=1}^N \varepsilon_i^2(k) p_i(k) - \hat{\sigma}^2 \right) - \lambda_2 \left( \sum_{i=1}^N p_i(k) - 1 \right). \quad (19)$$

The maximum is defined by  $\partial J / \partial p_i(k) = 0$  for  $i = 1, \dots, N$  and  $\partial J / \partial \lambda_j(k) = 0$  for  $j = 1, 2$ , which yields

$$\ln p_i(k) + 1 - \lambda_1 \varepsilon_i^2(k) - \lambda_2 = 0 \quad (20)$$

and the resulted probability  $p_i(k)$  is computed as

$$p_i(k) = \exp(-1 + \lambda_1 \varepsilon_i^2(k) + \lambda_2) = c_0 \cdot \exp(\lambda_1 \varepsilon_i^2(k)). \quad (21)$$

According to the constraint on the sum of the probability, the probability  $p_i(k)$  needs to be normalized as (22) such that the constant  $c_0$  can be canceled

$$p'_i(k) = \frac{\exp(\lambda_1 \varepsilon_i^2(k))}{\sum_{i=1}^N \exp(\lambda_1 \varepsilon_i^2(k))}. \quad (22)$$

Given the prediction error based on the criterion  $i$  ( $i = 1, 2, \dots, N$ ),  $\lambda_1$  is a common property of  $p(\varepsilon_i^2|i)$ , which is the the probability density function of  $\varepsilon_i^2$ . These probability density functions satisfy

$$\int_0^\infty p(\varepsilon_i^2|i) d(\varepsilon_i^2) = 1 \quad (23)$$

such that 1)  $p(\varepsilon_i^2|i)$  is the exponential distribution and 2) it is independent of the criterion and therefore is the same for all  $i$ . Since  $\lambda_1 = -1/\sigma_1^2$ , we can set  $\sigma_1^2 = \hat{\sigma}^2$  to obtain

$$p(\varepsilon_i^2|i) = \frac{1}{\hat{\sigma}^2} \exp\left(-\frac{\varepsilon_i^2}{\hat{\sigma}^2}\right). \quad (24)$$

#### REFERENCES

- [1] E. R. Kandel, J. H. Schwartz, T. M. Jessell, S. A. Siegelbaum, and A. J. Hudspeth, *Principles of Neural Science*, 5th ed. New York: McGraw-Hill, 2012.
- [2] D. Purves *et al.*, *Neuroscience*, 5th ed. Sunderland, MA: Sinauer, 2011.
- [3] J. Soechting, C. Buneo, U. Herrmann, and M. Flanders, "Moving effortlessly in three dimensions: Does Donders' law apply to arm movement?," *J. Neurosci.*, vol. 15, no. 9, pp. 6271–6280, 1995.
- [4] M. Latash, "Motor synergies and the equilibrium-point hypothesis," *Motor Control*, vol. 14, no. 3, p. 294C322, 2010.
- [5] M. H. Raibert and J. K. Hodgins, "Legged robots," in *Biological Neural Networks in Invertebrate Neuroethology and Robotics*, R. D. Beer, T. McKenna, and R. Ritzmann, Eds. New York: Elsevier, 1993, pp. 319–354.
- [6] M. Turvey and S. Fonseca, "Nature of motor control: perspectives and issues," *Adv. Exp. Med. Biol.*, vol. 629, pp. 93–123, 2009.
- [7] M. Kawato, "Internal models for motor control and trajectory planning," *Curr. Opin. Neurobiol.*, vol. 9, no. 6, pp. 718–727, 1999.
- [8] D. Wolpert and Z. Ghahramani, "Computational principles of movement neuroscience," *Nat. Neurosci.*, pp. 1212–1217, 2000.
- [9] L. Sciacivco, "A dynamic solution to the inverse kinematic problem for redundant manipulators," in *Proc. IEEE Int. Conf. Robot. Autom.*, Raleigh, NC, Mar. 1987, vol. 4, pp. 1081–1087.
- [10] L. Sciacivco, "A solution algorithm to the inverse kinematic problem for redundant manipulators," *IEEE Trans. Robot. Autom.*, vol. 4, no. 4, pp. 403–410, Aug. 1988.
- [11] H. Asada and J. Granito, "Kinematic and static characterization of wrist joints and their optimal design," in *Proc. IEEE Int. Conf. Robot. Autom.*, St. Louis, MO, Mar. 1985, pp. 244–250.
- [12] T. Yoshikawa, "Dynamic manipulability of robot manipulators," in *Proc. IEEE Int. Conf. Robot. Autom.*, St. Louis, MO, Mar. 1985, pp. 1033–1038.
- [13] T. Yoshikawa, *Foundations of Robotics: Analysis and Control*. Cambridge, MA: MIT Press, 1990.
- [14] H. Kim, L. Miller, and J. Rosen, "Redundancy resolution of a human arm for controlling a seven DOF wearable robotic system," presented at the EMBC, Boston, MA, Aug. 2011.
- [15] T. Kang, J. He, and S. I. H. Tillery, "Determining natural arm configuration along a reaching trajectory," *Exp. Brain Res.*, vol. 167, pp. 352–361, 2005.
- [16] N. Hogan, "An organizing principle for a class of voluntary movements," *J. Neurosci.*, vol. 4, no. 2, pp. 2745–2754, 1984.
- [17] T. Flash and N. Hogan, "The coordination of arm movements: An experimentally confirmed mathematical model," *J. Neurophysiol.*, vol. 5, pp. 1688–1703, 1985.
- [18] Y. Uno, M. Kawato, and R. Suzuki, "Formation and control of optimal trajectory in human multijoint arm movement—Minimum torque-change model," *Biol. Cybern.*, vol. 61, pp. 89–101, 1989.

- [19] E. Nakano *et al.*, "Quantitative examinations of internal representations for arm trajectory planning: Minimum commanded torque change model," *J. Neurophysiol.*, vol. 81, no. 5, pp. 2140–2155, 1999.
- [20] C. M. Harris and D. M. Wolpert, "Signal-dependent noise determines motor planning," *Nature*, vol. 194, pp. 780–784, 1998.
- [21] E. Todorov and M. I. Jordan, "Optimal feedback control as a theory of motor coordination," *Nature Neurosci.*, vol. 5, pp. 1226–1235, 2002.
- [22] H. Miyamoto and M. Kawato, "Tops (task optimization in the presence of signal-dependent noise) model," *Syst. Comp. Japan.*, vol. 35, pp. 48–58, 2004.
- [23] A. Biess, D. Liebermann, and T. Flash, "A computational model for redundant human three-dimensional pointing movements: Integration of independent spatial and temporal motor plans simplifies movement dynamics," *J. Neurosci.*, vol. 27, pp. 13045–64, 2007.
- [24] H. Kim, Z. Li, D. Milutinovic, and J. Rosen, "Resolving the redundancy of a seven DOF wearable robotic system based on kinematic and dynamic constraint," in *Proc. IEEE Int. Conf. Robot. Automat.*, St. Paul, MN, 2012, pp. 305–310.
- [25] B. Kashi, I. Avrahami, J. Rosen, and M. Brand, "A bi-criterion model for human arm posture prediction," in *2012 World Congr. Med. Phys. Biomed. Eng.*, Beijing, China, May 2012, pp. 1–4.
- [26] A. Frisoli, C. Loconsole, R. Bartalucci, and M. Bergamasco, "A new bounded jerk on-line trajectory planning for mimicking human movements in robot-aided neurorehabilitation," *Robot. Auton. Syst.*, vol. 61, no. 4, pp. 404–415, 2012.
- [27] Z. Li, H. Kim, D. Milutinovic, and J. Rosen, "Synthesizing redundancy resolution criteria of the human arm posture in reaching movements," *Redundancy Robot Manipulators Multi-Robot Syst.*, vol. 57, pp. 201–240, 2013.
- [28] N. I. Badler and D. Tolani, "Real-time inverse kinematics of the human arm," *Presence*, vol. 5, no. 4, pp. 393–401, 1996.
- [29] Motion Genesis May 13, 2014 [Online]. Available: <http://www.motiongenesis.com/>
- [30] T. Kane and D. Levinson, *Dynamics: Theory and Applications*. New York: McGraw-Hill, 1985.
- [31] S. L. Roberts and S. K. Falkenberg, *Biomechanics: Problem Solving for Functional Activity*. St. Louis, MO: Mosby, 1992.
- [32] Aerospace medical research laboratory, Investigation of inertial properties of human body Tech. Rep., 1975.
- [33] Z. Li, J. Roldan, D. Milutinovic, and J. Rosen, "The rotational axis approach for resolving the kinematic redundancy of the human arm in reaching movements," in *Proc. 35th Annu. Int. Conf. IEEE Eng. Med. Biol. Soc.*, Osaka, Japan, Jul. 2013, pp. 2507–2510.
- [34] Y. Wada, Y. Kaneko, E. Nakano, R. Osu, and M. Kawato, "Quantitative examinations for multi joint arm trajectory planning using a robust calculation algorithm of the minimum commanded torque change trajectory," *J. Neural Netw.*, vol. 14, pp. 381–393, 2001.
- [35] R. P. Duma and P. L. Strick, "Motor areas in the frontal lobe of the primate," *Physiol. Behav.*, vol. 77, pp. 677–682, 2002.
- [36] M. Graziano, C. Tylor, and T. Moore, "Complex movements evoked by micro stimulation of precentral cortex," *Neuron*, vol. 34, pp. 841–851, 2002.
- [37] F. E. Mount, M. Whitmore, and S. L. Stealey, Evaluation of neutral body posture on shuttle mission sts-57 (spacehab-1) Tech. Rep., 2003.
- [38] E. T. Jaynes, "Information theory and statistical mechanics," *Phys. Rev.*, vol. 106, pp. 620–630, 1957.



**Zhi Li** received the B.Sc. degree in mechanical engineering from China Agricultural University, Beijing, China, in 2006, the M.A.Sc. degrees in mechanical engineering from University of Victoria, Victoria, BC, Canada, in 2009, and the Ph.D. degree in computer engineering from University of California, Santa Cruz, CA, USA, in 2014.

She is a postdoc at Intelligent Motion Lab, Department of Electrical and Computer Engineering, Duke University, Durham, NC, USA. Her research interests focus on wearable robotics, surgical/rehabilitation robotics, teleoperation, haptics and virtual reality, neuromuscular control and stroke rehabilitation.



**Dejan Milutinovic** (M'11) received the Dipl.-Ing and Magister's degrees in electrical engineering from the University of Belgrade, Serbia, in 1995 and 1999, respectively, and a doctoral degree in electrical and computer engineering from Instituto Superior Técnico, Lisbon, Portugal, in 2004.

From 1995 to 2000, he worked as a Research Engineer in the Automation and Control Division of Mihajlo Pupin Institute, Belgrade, Serbia. He is currently an Associate Professor in the Department of Computer Engineering, University of California, Santa Cruz, CA, USA. His research interests are in the area of modeling and control of stochastic dynamical systems applied to robotics. He is an Associate Editor of the *ASME Journal of Dynamic Systems, Measurement, and Control*.

Dr. Milutinovic won the NRC award of the US Academies in 2008 and Hellman Fellowship in 2012. His doctoral thesis was the first runner-up for the best Ph.D. thesis of European Robotics by EURON, in 2004.



**Jacob Rosen** received the B.Sc. degree in mechanical engineering, M.Sc. and Ph.D. degrees in biomedical engineering from Tel-Aviv University, Tel-Aviv, Israel, in 1987, 1993, and 1997, respectively.

He is a Professor of medical robotics at the Department of Mechanical and Aerospace Engineering, University of California, Los Angeles, Los Angeles, CA, USA. His research interests focus on medical robotics, biorobotics, human centered robotics, surgical robotics, wearable robotics, rehabilitation robotics, neural control, and human-machine interface. From 1987 to 1992, he served as an officer in the IDF studying human-machine interfaces. From 1993 to 1997, he was a Research Associate developing and studying the EMG-based powered Exoskeleton at the Biomechanics Laboratory, Department of Biomedical Engineering, Tel-Aviv University. From 1997 to 2000, he was a Post-Doc at the Departments of Electrical Engineering and Surgery, University of Washington. From 2001 to 2008, he was a faculty member at the Department of Electrical Engineering, University of Washington with adjunct appointments with the Departments of Surgery. From 2008 to 2013, he served as a faculty member at the Department of Computer Engineering, University of California, Santa Cruz.